Error Quantification of the Axial Nodal Diffusion Kernel of the DeCART Code

Jin-Young Cho*, Kang-Seog Kim and Chung-Chan Lee
Korea Atomic Energy Research Institute, 150 Deokjin-dong, Yuseong-gu, Daejeon, 305-353, Korea

Abstract

This paper is to quantify the transport effects involved in the axial nodal diffusion kernel of the DeCART code. The transport effects are itemized into three effects, the homogenization, the diffusion, and the nodal effects. A five pin model consisting of four fuel pins and one non-fuel pin is demonstrated to quantify the transport effects. The transport effects are analyzed for three problems, the single pin (SP), guide tube (GT) and control rod (CR) problems by replacing the non-fuel pin with the fuel pin, a guide-tube and a control rod pins, respectively. The homogenization and diffusion effects are estimated to be about -4 and -50 pcm for the eigenvalue, and less than 2 % for the node power. The nodal effect on the eigenvalue is evaluated to be about -50 pcm in the SP and GT problems, and +350 pcm in the CR problem. Regarding the node power, this effect induces about a 3 % error in the SP and GT problems, and about a 20 % error in the CR problem. The large power error in the CR problem is due to the plane thickness, and it can be decreased by using the adaptive plane size. From the error quantification, it is concluded that the homogenization and the diffusion effects are not controllable if DeCART maintains the diffusion kernel for the axial solution, but the nodal effect is controllable by introducing the adaptive plane size scheme.

KEYWORDS: DeCART, Transport Effect, Homogenization Effect, Diffusion Effect, Nodal Effect, Error Quantification

1. Introduction

The DeCART (Deterministic Core Analysis based on Ray Tracing) code [1] is a whole core neutron transport code capable of a direct sub-pin level flux calculation for a power generating condition of a PWR core. Regarding the 3-D heterogeneous whole core transport calculation, an innovative transport calculation scheme involving the planar method of characteristics (MOC) [2] and the 3-D coarse mesh finite difference (CMFD) [3] formulation is used. In this scheme the MOC solution provides the cell-homogenized group constants and the radial coupling coefficients which correct the surface current by the two node-averaged fluxes. In the 3-D CMFD formulation, the axial dependency of the flux is represented by the diffusion theory and it is resolved by the nodal expansion method (NEM) [4]. The axial leakage determined at each plane by the NEM

* Corresponding author, Tel. 82-42-868-8954, Fax. 82-42-868-8990, E-mail: jyoung@kaeri.re.kr

solution is then provided for the planar MOC problem as a source so that the consistency between the planar MOC and 3-D CMFD problems is retained as far as the neutron balance is concerned.

The axial NEM based nodal diffusion solution for the homogenized node is an approximate one to the fine-mesh transport solution for the heterogeneous three-dimensional node. Therefore, the axial solution of the DeCART code inevitably contains the errors associated with these approximations which are expected to be larger for an axially heterogeneous problem. The errors associated with the two-group nodal diffusion calculation are well itemized into four effects in reference [5]: (1) a homogenization effect, (2) a special discretization effect, (3) a group condensation effect, and (4) a transport effect. In these four effects, the group condensation effect is not relevant to the axial kernel of the DeCART code, because the axial kernel uses the same energy group structure as the radial MOC kernel. Therefore, in this paper the three effects related with the axial NEM solution are examined and quantified.

DeCART solves the axial NEM incorporated into the 2-D CMFD equation. The neutron balance equation for a 3-D node includes the net currents at the boundary surfaces. The net current, in the CMFD formulation, can be expressed by the node average flux of the neighboring nodes. To incorporate the axial NEM equation into the nodal balance equation, the net current equation should be derived from the NEM equation. The details will be described in Chapter 2. And then, the solution errors related to the axial kernel will be discussed in Chapter 3.

2. Nodal Expansion Method in the CMFD Formulation

DeCART solves a 3-D CMFD equation which combines the radial 2-D CMFD equation with the axial NEM equation. The neutron balance equation for a three-dimensional can be written as:

$$\frac{1}{h_r}\sum_{s=1}^{N_{rad}}\left(J_r^{+s}-J_r^{-s}\right)+\frac{1}{h_z}\sum_{s=1}^{N_{ax}}\left(J_z^{+s}-J_z^{-s}\right)+\Sigma_r\bar{\phi}=\frac{1}{k_{eff}}S_f+S_s+S_{ext}. \quad (1)$$

Here, h_r and h_z are the node size in the radial and the axial direction, J_r^s and J_z^s are the partial currents on the surface s in the radial and axial direction, and N_{rad} and N_{ax} are the number of surfaces in the radial and the axial direction respectively. Σ_r and $\bar{\phi}$ mean the removal cross section and the node averaged flux, and S_f, S_s and S_{ext} are the notations for the fission, scattering and the external neutron sources respectively. The superscripts ± designate the outgoing and incoming partial currents while T and B indicate the top and bottom surface of a node respectively. The first term of Eq. (1) is the total neutron loss through the radial surfaces, and it can be expressed by the node average fluxes when applying the conventional CMFD formulation. The second term of Eq. (1) is the total neutron loss through the axial surfaces, and it can be replaced by the node average flux and the partial currents from the NEM formulation.

2.1 Partial Current Formulation

By applying the conventional NEM, the outgoing partial current at a node surface can be derived in terms of the incoming partial currents, the node average flux and the flux moments as:

$$J_z^{+T}=T_1\,J_z^{-T}+T_2\,J_z^{-B}+T_3\,\bar{\phi}+T_4\,\tilde{\phi}_1+T_5\,\tilde{\phi}_2\,, \quad (2)$$

where

$$T_1 = \frac{1-960\beta^2}{(1+40\beta)(1+24\beta)}, \quad T_2 = \frac{-16\beta}{(1+40\beta)(1+24\beta)},$$

$$T_3 = \frac{20\beta}{(1+40\beta)}, \quad T_4 = \frac{30\beta}{(1+24\beta)}, \quad T_5 = -\frac{70\beta}{(1+40\beta)}.$$

Here $\widetilde{\phi}_1$ and $\widetilde{\phi}_2$ mean the first- and second-moments for the axial neutron flux respectively, and β is the ratio of the diffusion coefficient to the node size.

Also, the weighted residual equations for first and the second moments can be derived as:

$$\widetilde{\phi}_1 = N_1\left(J_z^{-T} - J_z^{-B}\right) + N_2\widetilde{S}_1 , \tag{3}$$

$$\widetilde{\phi}_2 = M_1\overline{\phi} + M_2\left(J_z^{-T} + J_z^{-B}\right) + M_3\widetilde{S}_2 , \tag{4}$$

where

$$N_1 = \frac{20\beta(1+T_1-T_2)}{20\beta(3-2T_4)+h_z\Sigma_r}, \; N_2 = \frac{h_z}{20\beta(3-2T_4)+h_z\Sigma_r},$$

$$M_1 = \frac{28\beta(1-2T_3)}{28\beta(5+2T_5)+h_z\Sigma_r}, \; M_2 = \frac{-28\beta(1+T_1+T_2)}{28\beta(5+2T_5)+h_z\Sigma_r}, \; M_3 = \frac{h_z}{28\beta(5+2T_5)+h_z\Sigma_r}.$$

Here $\widetilde{S}_1$ and $\widetilde{S}_2$ are the first and second moment sources respectively including not only the fission, the scattering and the external sources but also the transverse leakage source.

2.2 NEM Integrated CMFD Formulation

In Eq. (3), the first flux moment is not coupled with the other variables such as node average flux or the second moment. Therefore, Eq. (3) can be easily solved if the incoming partial currents and the first moment sources are given. However, the second moment in Eq. (4) is coupled with the node average flux, which requires another equation that couples the second moment and the node average flux, that is, the neutron balance equation.

The neutron balance equation of Eq. (1) can be expressed in terms of the node average flux, the incoming partial currents and the axial flux moments by using the outgoing partial current equation (2) and the second flux moment equation (4) as:

$$\begin{aligned} -\frac{1}{h}\sum_{s=1}^{N_{rad}^i}\left(\widetilde{D}^{i,s}+\hat{D}^{i,s}\right)\overline{\phi}^{i,s} + \left\{\Sigma_a^i + \frac{2T_3^i}{h_z} + \frac{1}{h}\sum_{s=1}^{N_{rad}^i}\left(\widetilde{D}^{i,s}-\hat{D}^{i,s}\right) + \frac{2T_5^i}{h_z}M_1^i\right\}\overline{\phi}^i \\ = \overline{S}^i - \left\{\frac{1}{h_z}\left(T_1^i+T_2^i-1\right)+\frac{2T_5^i}{h_z}M_2^i\right\}\left(J_z^{-i,T}+J_z^{-i,B}\right) - \frac{2T_5^i}{h_z}M_3^i\widetilde{S}_2^i, \end{aligned} \tag{5}$$

where $\overline{S}^i$ is the node average neutron source of a node *i* including the fission, the scattering and the external sources that are assumed to be available from the previous iteration step. Eq. (5) can construct a plane-wise 2-D CMFD problem and it can be solved if the boundary conditions are given. The boundary conditions of Eq. (5) include the incoming partial currents at the top and bottom surfaces, and the second moment source.

2.3 Solution Algorithm of the NEM Integrated CMFD Equation

If Eq. (5) is solved by the group-wise and the plane-wise iteration scheme, the incoming partial currents and the node average sources can be given as the boundary conditions by using the solutions for the other group and planes. However, the second moment source can not be given completely as the boundary condition due to the radial leakage source, which is same in the first moment source of Eq. (3). To resolve this problem exactly, the radial leakage term should be derived in terms of the node average fluxes of the neighboring nodes, and then moved to the left hand side (LHS) in Eq. (5), which results in a complicated form. In DeCART, to avoid this complication, the radial leakage sources for the first and the second moments are determined before solving Eq. (5) by using the solutions at the previous iteration step.

The one-group planar problem is solved by a Krylov subspace method employing the block-wise incomplete LU factorization preconditioner [7] which shows good convergence characteristics even with a small radial mesh size amounting to a pin cell. For each plane, the group-wise calculation is performed with the updated scattering source. After a few group sweepings, the axial boundary condition involving the incoming currents and the moments is updated. After the completion of the planar sweep, one outer iteration step is completed and the eigenvalue and the fission sources are updated accordingly.

2.4 The transport effect in the DeCART solution algorithm

DeCART performs the axial NEM calculation for a relatively large homogenized cell. Therefore, the transport effects relevant to the axial solution can be itemized into three effects, a cell homogenization, a diffusion, and a nodal effects. The cell homogenization effect can be quantified by the solution differences between for the homogeneous and the heterogeneous cells. For the quantification of the homogenization effect, the same transport calculation for the homogeneous cell as the heterogeneous cell should be performed by using the same ray tracing parameters such as the number of angles and the ray spacing. The only differences are the geometry and the cross sections. The homogeneous transport calculation uses the cross sections generated from the heterogeneous transport calculation. If the homogeneous group constants are generated to conserve the neutron current at the node surfaces by the equivalence theory, the homogeneous transport calculation reproduces the results of the heterogeneous transport calculation. However, because DeCART can not use the equivalent homogeneous group constants for the axial direction, a little bit errors exist in the transport calculation for the homogeneous cell.

The diffusion effect can be quantified by the differences between the transport and the diffusion solutions for the homogenized cell. The diffusion solutions should be obtained by using the same cross sections as used in the transport solution. In the diffusion calculation, the diffusion constant is obtained from the transport cross section of the transport calculation by using the P1 scattering approximation. The true diffusion solution can not be obtained for a multi-group and a multi-region eigenvalue problem. In this analysis, the best diffusion solutions are obtained by using the ultra-fine mesh finite difference method (FDM).

Similarly, the nodal effect can be quantified by the differences between the nodal and the reference diffusion solutions. For the nodal calculation, the multi-group cross sections should be generated by using the reference diffusion solution. However, in the normal DeCART calculation, the cross sections for the axial NEM calculation are generated for a thick plane size by using the radial MOC solution because the axial fine-mesh diffusion calculation is not performed. Therefore,

in this paper, an approximate cross section which will be described in the next chapter is used for the axial NEM calculation instead of the rigorous multi-group cross sections.

3. Computational Results

Fig. 1 shows the base model for the quantification of the axial transport effect. This model consists of 5 pins, and it uses reflective boundary conditions except for the top surface where the vacuum boundary condition is imposed. Four pins, pins 1, 2, 4 and 5, are the fuel pins and pin 3 is a non-fuel pin. The fuel pin model is demonstrated by chopping a fuel pin axially at the fuel centerline. The demonstrated model is similar to the slab geometry model but for the additional reflector region at the top and bottom of the fuel pins. The equivalent fuel radius is determined to preserve the fuel volume. The non-fuel pin of pin 3 is to analyze the perturbation effect of the water hole or the control rod. This 5-pin model can be simply converted to a single fuel pin model by replacing the non-fuel pin with the same fuel pin.

Figure 1: Base Model for the Analysis of the Transport Effect

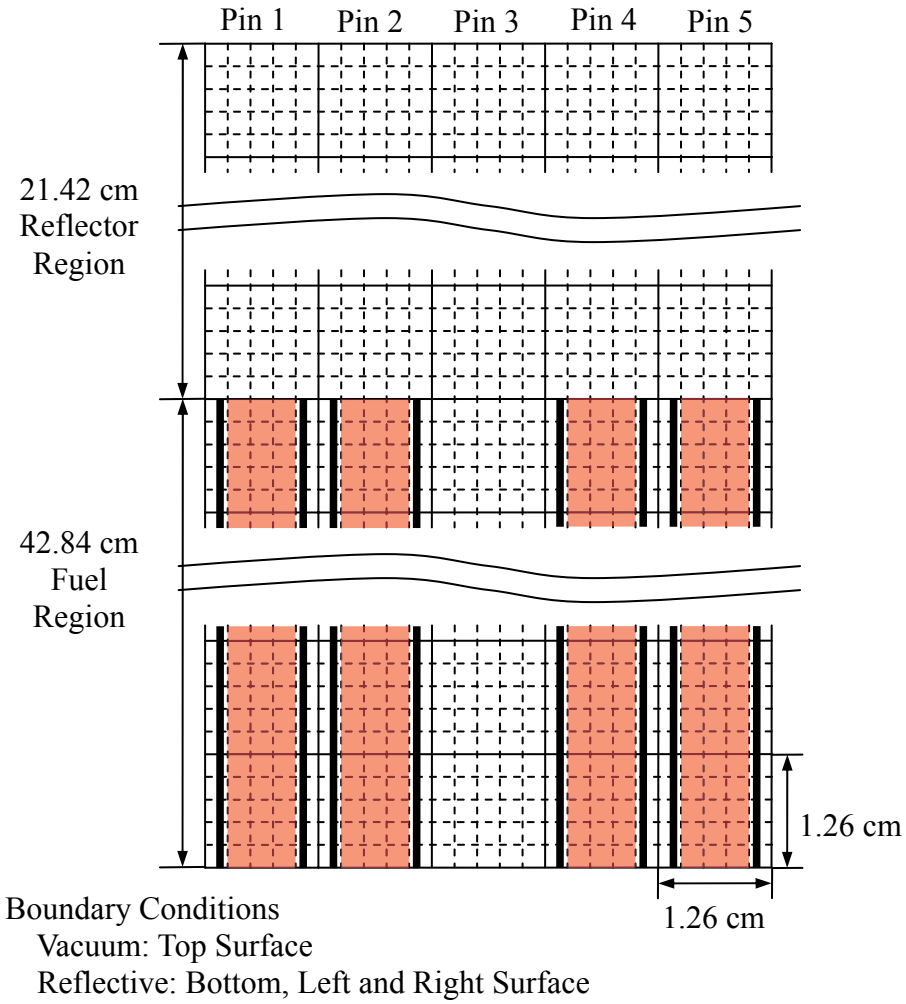

The three reference problems are solved by the DeCART code, the single pin problem (problem SP), the normal problem by replacing the non-fuel pin with a guide tube pin (problem GT), and the rodded problem by using the control rod (problem CT). The transport effect can be quantified exactly in the SP problem because this problem is free from the error resulting from a radial coupling between the pins. In the other two problems, the radial coupling errors exist due to a geometrical perturbation from the guide tube or control rod pins. Therefore, the other problems can produce an approximate transport effect. In all the calculations, the DeCART code is used with the refined ray parameters of a 0.2 mm ray spacing and 8 azimuthal and 4 polar angles for the octant solid space. Also, in the transport calculation, the square cell is divided into 25 flat source regions which are depicted by the dashed-line in Fig. 1. The geometrical and the cross section data are obtained from the C5G7 rodded benchmark problem [6].

Table 1: Notations for the Calculation

Notations	Geometrical Modeling	Neutronics	Dimension	Method	
				Radial	Axial
HetTr2D	Heterogeneous	Transport	2D	MOC	NA
HomTr2D	Homogeneous	Transport	2D	MOC	NA
HomDif2D	Homogeneous	Diffusion	2D	FDM	NA
HetTr3DFD	Heterogeneous	Transport	3D	MOC	FDM
HetTr3DNodal	Heterogeneous	Transport	3D	MOC	Nodal

Table I shows the computations that are performed to examine the transport effect. Computation of HetTr2D which deals with the exact heterogeneous geometry of Fig. 1 is for the reference solution. The cell-based homogenized group constants are generated for the homogeneous transport calculation and the homogeneous diffusion calculation during this computation. Computation of HomTr2D which uses the cell-based homogenized constants is performed to estimate the homogenization effect which can be estimated by the solution difference between HetTr2D and HomTr2D. Computation of HomDif2D which also uses the cell-based homogenized constants is performed to estimate the diffusion effect which can be estimated by the solution difference between HomTr2D and HomDif2D. Computations of HetTr3DFD and HetTr3DNodal are performed to estimate the nodal effect. The rigorous nodal effect for Fig. 1 can be estimated by performing the two-dimensional nodal diffusion calculation with the node-wise homogenized cross sections which can be produced from HomDif2D. In this case, an additional nodal program is required for the nodal diffusion calculation. Therefore, computations of HetTr3DFD and HetTr3DNodal are performed to avoid this complication by using the DeCART code. The geometrical model for both computations can be easily achieved by modifying the X-Y model of Fig.1 to the X-Z model and extending the Y-mesh to the cell size and by using the reflective conditions at the radial boundaries. Computation of HetTr3DFD can produce exactly the same solution if the true 3-D transport calculation is applied with the same polar angles as the azimuthal angles. However, the radial transport and the axial diffusion calculation which are actually performed in the DeCART code can only produce an approximate solution of the HetTr2D. The difference in the geometrical model between the HetTr3DFD and HetTr3DNodal computations is

in the axial plane size. The fine axial mesh size of 2.6775 cm is used for HetTr3DFD and it is 10.71 cm for HetTr3DNodal. In both computations, NEM is used for the axial solution, which can produce an almost exact solution with the axial mesh size of 2.6775 cm. Computation of HetTr3DNodal is the real calculation of the DeCART code for the 3-D problem, which is another reason why this model was the final selection. The nodal effect is estimated by the solution difference between HomTr2D and HomDif2D. In these five computations, four computations except for HomDif2D are performed by using the DeCART code. Computation of HomTr2D is performed by using the ultra-fine mesh which divides a cell into 7x7 subsections to produce an exact diffusion solution for the homogenized cell.

Table 2 shows the transport effects on the eigenvalue. The two effects except for the nodal effect will be discussed first. The homogenization effect is estimated to be about 4 pcm which seems trivial. The diffusion effect is estimated to be about -52 pcm in the SP problem. Computation of HetTr3DFD involves both the homogenization and the diffusion effects. The net effect is estimated to be about -45 pcm which is similar with that from HomTr2D and HomDif2D, which means that the computation HetTr3DFD can be used effectively to estimate the net effect. In the GT problem, the net effect turned out to be about -36 pcm. However, in the CR problem, the net effect is doubled due to the rod effect. In the rodded plane, the axial flux shape varies heavily, so the plane size needs to be minimized. A little bit larger net effect in the CR problem indicates that the axial mesh size of 2.6775 cm is not small enough. However, the axial mesh size of 2.6775 cm can not be decreased due to the limitation of the current DeCART version.

Table 2: Transport Effects on k_{eff} of the DeCART Code

CASE	Calculation	k_{eff}	Effects, pcm	Comments
SP	HetTr2D	1.27184	-	
	HomTr2D	1.27190	4.1	Homogenization Effect
	HomDif2D	1.27106	-52.4	Diffusion Effect
	HetTr3DFD	1.27111	-45.2	Homogenization + Diffusion
	HetTr3DNodal	1.27022	-55.3	Nodal Effect
GT	HetTr2D	1.27186	-	
	HetTr3DFD	1.27128	-36.2	Homogenization + Diffusion
	HetTr3DNodal	1.27040	-54.3	Nodal Effect
CR	HetTr2D	1.18144	-	
	HetTr3DFD	1.18989	-109.0	Homogenization + Diffusion
	HetTr3DNodal	1.19496	356.2	Nodal Effect

Fig. 2 and 3 show the power distributions for the three problems. In the SP problem, all the power distributions are very close. However, in the vicinity of the top reflector, the power distributions using the homogenized cross sections show a little bit difference from the heterogeneous solution. Power distributions by using the homogenized cross sections are very close to each other. Regarding the power distribution of HetTr3DFD, it follows the power distributions of the computation of HetTr2D very well.

Figure 2: Relative Power Distribution for SP Problem

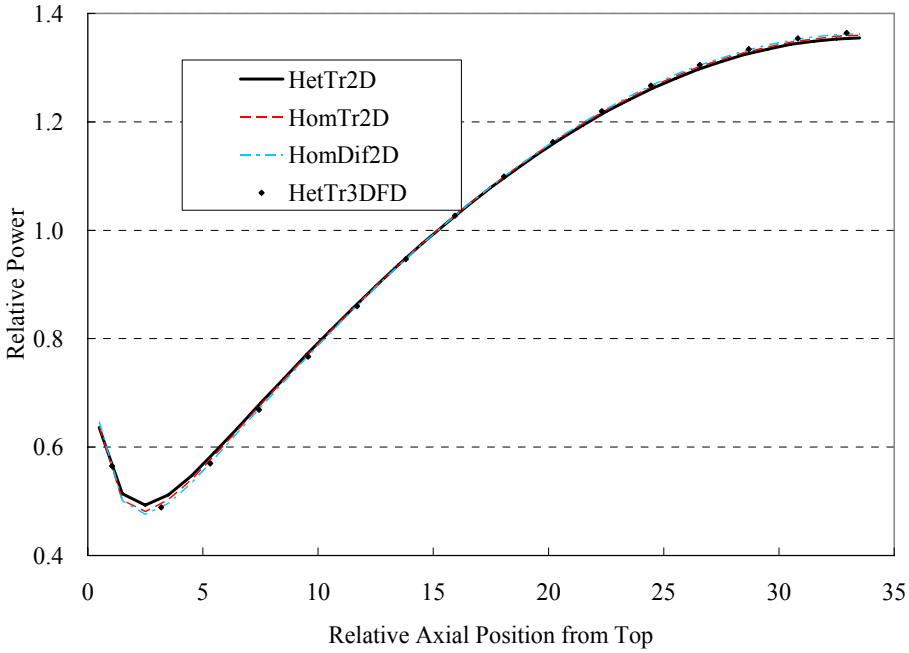

Figure 3: Relative Power Distribution for GT and CR Problems

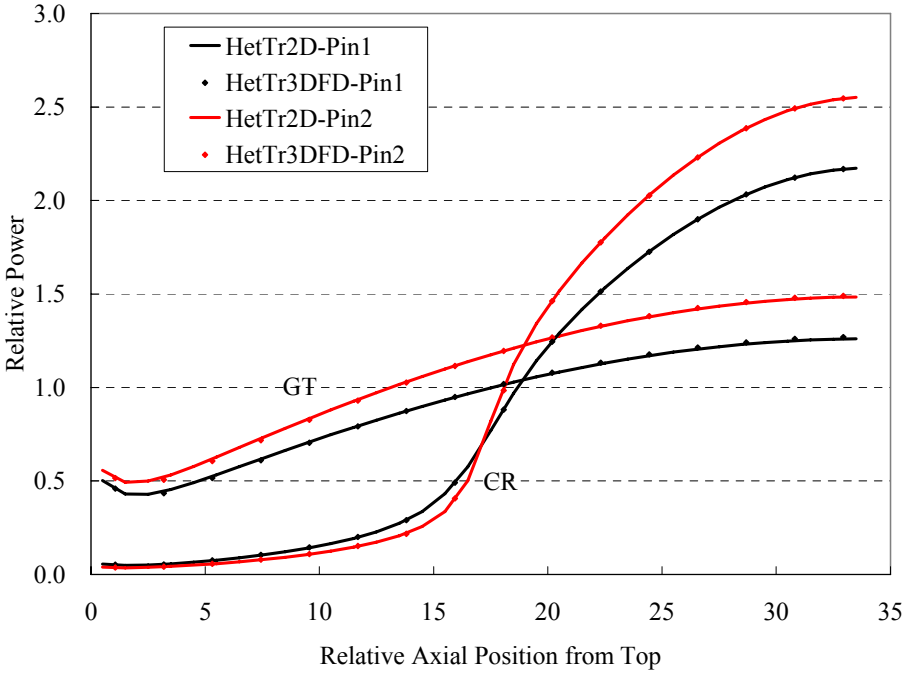

Fig. 4 shows the transport effects on the node power. The net homogenization and diffusion effects are estimated to be about a 2 % error in all the problems. However, the nodal effect induces

about a 3 % error in the SP and GT problems, and about a 20 % error in the CR problem. In Table 2, the nodal effect also induces large errors on the eigenvalue showing about -50 pcm in the SP and GT problems and about +350 pcm in the CR problem which is beyond the acceptable range. This nodal effect can be decreased dramatically by reducing the plane size or by using an adaptive plane size. As shown in Fig. 3, the power shape alters at the interface between the rodded and unrodded planes. Therefore, the plane sizes in the vicinity of this interface need to be decreased. Fig. 5 shows the plane size effect of the interface rodded plane. In this examination, the total thickness and the number of rodded planes are fixed, which means that a reduced thickness of the interface plane is used to increase the thickness of the other rodded plane. Fig. 5 indicates that the eigenvalue and power errors decrease dramatically by reducing the interface plane size and about 7 cm of the interface plane size produces similar nodal effects to the SP or GT problems. Fig. 5 also indicates that the nodal effects are controllable with the adaptive plane thickness.

Figure 4: Transport Effect on the Nodal Power

0.585	0.515	0.598	0.071	0.054	
-1.03					
-1.59	-2.03	-1.92	0.21	-0.27	
-3.36	-3.17	-3.20	-18.9	-19.6	
0.902	0.832	0.976	0.283	0.223	
-0.05					
-0.26	-0.24	-0.19	-0.48	-0.92	
-0.03	-0.21	-0.15	-2.04	-2.37	
1.183	1.098	1.289	1.341	1.289	
+0.22					
+0.37	+0.34	+0.34	-0.02	-0.12	
+0.65	+0.59	+0.58	+2.24	+2.37	
1.330	1.238	1.454	2.053	1.454	← Reference Power
+0.32					← Hom. Effect (% Err)
+0.56	+0.65	+0.63	+0.12	+0.11	← Hom. & Diff. Eff. (% Err)
+0.88	+0.80	+0.84	-0.64	-0.68	← Nodal Effect (% Err)
Pin 1	Pin 1	Pin 2	Pin 1	Pin 2	
(a) Problem SA	(b) Problem GT		(c) Problem CR		

4. Conclusion

The transport effects were quantified by using the demonstrated 5 pin model. From the error quantification, it was concluded that the homogenization and the diffusion effects among the transport effects were not controllable if DeCART maintains the diffusion kernel for the axial solution, but the nodal effect which would induce a large error was controllable by introducing the adaptive plane size scheme.

Acknowledgements

This work was supported by the International Nuclear Energy Research Initiative (INERI) problem jointly funded by the Ministry of Science and Technology of Korea and the Department of Energy of the United States.

References

1) J. Y. Cho, H. G. Joo, K. S. Kim, S. Q. Zee. And M. H. Chang, "Three-dimensional heterogeneous whole core transport calculation employing planar MOC Solution," Trans. Am. Nucl. Soc., **87**, 234, Washington, DC, USA, Nov. 17-21 (2002).
2) M. J. Halsall, "CACTUS, a characteristics solution to the neutron transport equations in complicated geometries," AEEW-R-1291, UKAEA, Winfrith (1980).
3) T. M. Sutton, "NODEX: A higher order NEM-based nodal code," Proc. Topical Meeting on Advances in Nuclear Engineering Computation and Radiation Shielding, 38:1-38:11, Santa Fe, New Mexico, USA, Apr. 9-13 (1989).
4) H. Finnemann, F. Bennewitz and M. R. Wagner, "Interface nodal current technique for multi-dimensional reactor calculation," Atomkernenergie, **30**, 123 (1977).
5) T. Downar, C. H. Lee and G. Jiang, "An assessment of advanced nodal methods for MOX fuel analysis in light water reactors," Proc. PHYSOR'2000, May 7-12, Pittsburgh, PA, USA (2000).
6) M. A. Smith, G. Palmiotti, T. A. Taiwo, E. E. Lewis and N. Tsoulfanidis, "Benchmark specification for deterministic MOX fuel assembly transport calculations without special homogenization (3-D Extension C5G7 MOX), OECD/NEA Report, NEA/NSC/DOC(2006)6.
7) H. G. Joo and T. J. Downar, "An Incomplete Domain Decomposition Preconditioning Method for Nonlinear Nodal Kinetics Calculation," Nucl. Sci. Eng., **123**, 403 (1996).

Figure 5: Transport Effect with the Thickness of the Interface Plane